The growth and erosion of cinder cones in Guatemala and El Salvador: Models and statistics

Karen Bemis [a,*], Jim Walker [b], Andrea Borgia [a,d], Brent Turrin [a], Marco Neri [c], Carl Swisher III [a]

[a] Department of Earth and Planetary Science, Rutgers, The State University of New Jersey, Piscataway, NJ 08855, USA
[b] Department of Geology and Environmental Geosciences, Northern Illinois University, DeKalb, IL 60115, USA
[c] Instituto Nazionale di Geofisica e Vulcanologia, Piazza Roma, 2, 95123 Catania, Italy
[d] Department of Earth and Environmental Sciences, The Open University, Walton Hall, Milton Keynes, MK7 6AA, UK

ARTICLE INFO

ABSTRACT

Morphologic data for 147 cinder cones in southern Guatemala and western El Salvador are compared with data from the San Francisco volcanic field, Arizona (USA), Cima volcanic field, California (USA), Michoácan–Guanajuato volcanic field, Mexico, and the Lamongan volcanic field, East Java. The Guatemala cones have an average height of $110 +/- 50$ m, an average basal diameter of $660 +/- 230$ m and an average top diameter of $180 +/- 150$ m. The general morphology of these cones can be described by their average cone angle of slope $(24 +/- 7)$, average height-to-radius ratio $(0.33 +/- 0.09)$ and their flatness $(0.24 +/- 0.18)$. Although the mean values for the Guatemalan cones are similar to those for other volcanic fields (e.g., San Francisco volcanic field, Arizona; Cima volcanic field, California; Michoácan–Guanajuato volcanic field, Mexico; and Lamongan volcanic field, East Java), the range of morphologies encompasses almost all of those observed worldwide for cinder cones.

Three new ^{40}Ar/^{39}Ar age dates are combined with 19 previously published dates for cones in Guatemala and El Salvador. There is no indication that the morphologies of these cones have changed over the last 500–1000 ka. Furthermore, a re-analysis of published data for other volcanic fields suggests that only in the Cima volcanic field (of those studied) is there clear evidence of degradation with age.

Preliminary results of a numerical model of cinder cone growth are used to show that the range of morphologies observed in the Guatemalan cinder cones could all be primary, that is, due to processes occurring at the time of eruption.

© 2010 Elsevier B.V. All rights reserved.

1. Introduction

The eruption mechanisms of cinder cones have long been studied for their influence on the growth of the cones themselves (e.g., Porter, 1972; McGetchin et al., 1974; Settle, 1979). Early studies assumed that all cinder cones were formed by the same Strombolian (bubble-bursting) eruptions as observed for the cinder cones at the summits of Mount Etna and Stromboli (Chouet et al., 1974; McGetchin et al., 1974; Favalli et al., 2009). More recent studies have recognized that most of the historical eruptions forming cinder cones in monogenetic volcanic fields have actually been column-forming eruptions akin to plinian eruptions although not quite as energetic (e.g., Parícutin as described in Luhr and Simkin, 1993; see also the review in Riedel et al., 2003). These mechanisms may have a strong influence on grain size and fragmentation (since volatile content and lava chemistry may differ) and also on the proportion of the magma that ends up in the cinder cone. However, laboratory studies and numerical models suggest that there is little difference in the final cone morphology (Riedel et al., 2003). In both cases, material is initially deposited very near the crater rim and then cascades down slope. So the size of the cone is a function of the amount of magma erupted less the amount transported to the neutrally buoyant volcanic cloud (which is then advected by winds away from the cone). Likewise, in both cases, the morphology of the cone is a function of the landslide processes; thus studies (e.g., Wood, 1980a,b; Dohrenwend et al., 1986) have concluded that all pristine cones should have a similar angle of slope (equal to the angle of repose for scoria, usually assumed to be 33°).

A brief review of historical eruptions suggests at least one fallacy in this view: not all historical cones approach an average angle of slope of 33° (Table 1), which implies either the angle of repose varies between cones or not all cones have angles of slope at the angle of repose. Later, we will present evidence that the earliest phase of growth involves building up the flanks until they are at the angle of repose. Also, it is unlikely that the angle of repose is a universal constant; both median (or average) grain size and angularity of clasts vary over a sufficient range to affect the angle of repose (Bemis and Bonar, 1997; Cohen and Bemis, 1998; Riedel et al., 2003). Thus when lower angles of slope are observed in older cones, it cannot be simply assumed that they are eroded.

* Corresponding author. Department of Earth and Planetary Sciences, Rutgers University, 610 Taylor Road, Piscataway, NJ 08854, USA.
E-mail address: bemis@rci.rutgers.edu (K. Bemis).

Table 1
Angles of slope and eruption data for several cinder cones erupting in historical times.

Cone name	Eruption dates	Eruption duration	Cone volume	Cone angle of slope[a]	Reference
Paricutin, Mexico	1943–1952	9 years	3.26×10^8 m^3	30° (30°–33°)	Luhr and Simkin (1993)
Cono del Laghetto, Etna	July 19–Aug 6, 2001	18 days	$4.61 (+/-0.17) \times 10^6$ m^3	24° (9°–22°)[b]	Fornaciai et al. (2010), this paper
Southern Cone 1, Tolbachik, Kamchatka	July 6–October 7, 1975	93 days	3.54×10^8 m^3	25°	Fedotov and Markhinin (1983)
Southern Cone 2, Tolbachik, Kamchatka	August 9–October 7, 1975	59 days	1.78×10^7 m^3	34° (23°–38°)	Fedotov and Markhinin (1983)
Southern Cone 3, Tolbachik, Kamchatka	August 16–25, 1975	9 days	1.93×10^8 m^3	27° (27°–31°)	Fedotov and Markhinin (1983)
Oldonyio Lengai	June 13, 2007–June 23, 2008	1 year	6.63×10^6 m^3	24° (10°–29°)	Matthieu Kervyn, unpublished data

[a] The reported cone angle of slope is the final average angle of slope and, in parentheses, the range of average angles of slope observed during growth of the cone. The average angles of slope are calculated from height, basal diameter and top diameter.
[b] The upper flank slopes of Cono del Laghetto were 29°–31° in the final cone (Fornaciai et al., 2010).

This study presents two kinds of data: (1) a statistical analysis of the population of cinder cones existing today in the volcanic fields of Guatemala and western El Salvador (GSVF) (along with several other populations of cinder cones for comparison) and (2) a look at the variations in GSVF cinder cones over time (again along with similar data from other regions for comparison). We will start by reviewing our definitions of the morphologic parameters used to describe cinder cones both to provide clarity in interpretation and to introduce some non-standard presentations used herein. We then describe the population of cinder cones in GSVF as well as their geologic context. Following is a comparison with cinder cones from other regions of the world. Finally, we discuss the implications for models of cinder cone growth and erosion and present some preliminary results from a numerical model.

1.1. Morphological measurements

Like most previous studies (e.g., Wood, 1980a; Dohrenwend et al., 1986; Hooper and Sheridan, 1998; Favalli et al., 2009), we characterize the gross morphology of a cinder cone by measuring its basal diameter (2r), its height (h), and its top diameter (2t). Both the basal and top diameters are defined by a break in slope and the line describing either is allowed to cross contours (i.e., not constrained to a single elevation). The top diameter will correspond to the crater diameter when a crater is present; it will not necessarily be zero when there is no discernable crater as there may still be a break in slope and a flatter top region (Fig. 1). The height is an average of the elevation difference for each flank, which is similar to the methodology proposed by Favalli et al. (2009) but was based on techniques developed for seamounts (Smith and Cann, 1992). Angles of slope (which are not the maximum angle of slope on the cones) were not measured directly but are calculated as:

$$\text{angle of slope} = arctan(h / (r-t)).$$

Volumes are similarly calculated by:

$$V = (1/3)\pi(h)\left(r^2 + r*t + t^2\right).$$

The three basic measures were combined in a number of ways, including angle of slope, flatness (=t/r) and height-to-radius ratio (=h/r). Principal component analysis suggested that three combinations best described the overall variance: height-to-radius ratio, flatness and some measure of size (Bemis, 1995). Volume, basal diameter and height all work equally well as a measure of size but only one is needed. Bemis (1995) noted that the angle of slope is not as good a descriptor of variance as the height-to-radius ratio; for this reason, we will tend to emphasize height-to-radius ratios over angles of slope in the statistical discussions later. Measurements were made on topographic maps at a scale of 1:50,000 with a contour interval of 20 m. Errors in the angle of slope calculations are estimated at ~5° (based on measurement errors of 10-20 m in height and of 50-100 m in basal

diameter). Errors in height-to-radius ratio calculations are estimated at ~0.04. Errors in flatness are estimated at ~0.02.

2. The cinder cones of Guatemala and western El Salvador

Volcanoes of the Guatemalan–Salvadoran volcanic field (GSVF) follow the general trend of the Central American Volcanic Front, which is roughly parallel to the Central American Trench (Fig. 2). In this paper, we are concerned only with the cinder cones, which are small volcanoes built by
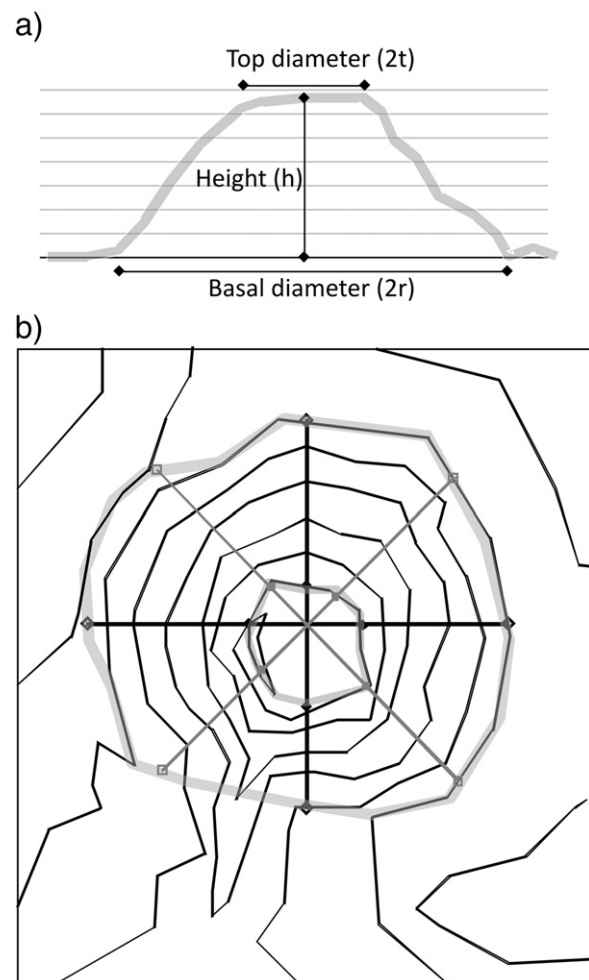

Fig. 1. Measuring the morphology of a cinder cone: (a) the cross-section shows schematically how the height, basal diameter and top diameter relate to the cone profile. (b) On the map view, the broad light gray bands show the interpreted position of the base and the top. The diameter of each is measured in four orientations (both black and gray bars) and averaged; the height is measured as the elevation difference over each of the four quadrants (black bars) and averaged.
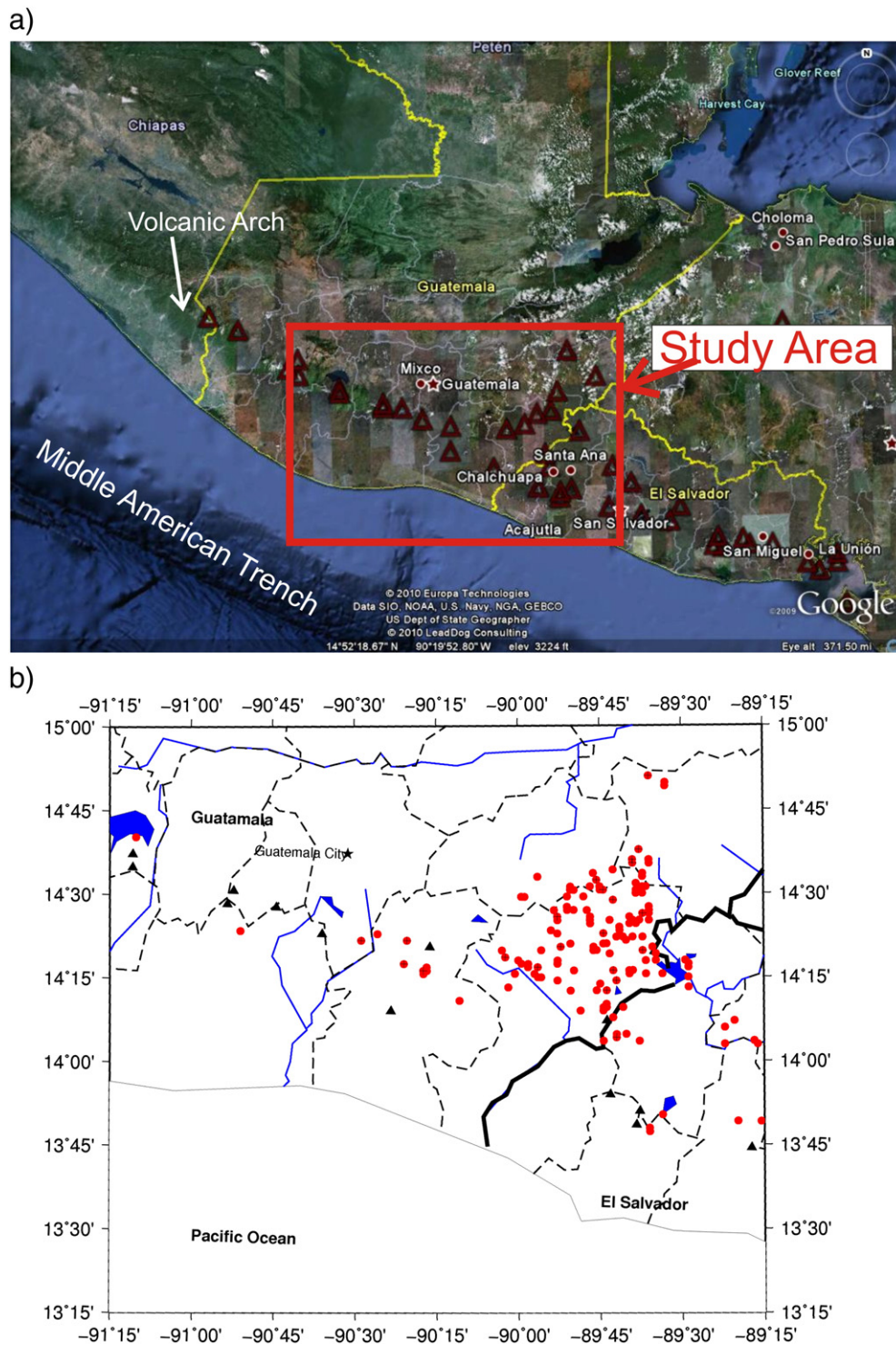
a)

b)

Fig. 2. The cinder cones of Guatemala and western El Salvador (GSVF) are distributed along and behind the Central American Arc. The majority of cinder cones are found behind the arc on the region of the Ipala Graben near the border between the two countries. Faint black crosses on top of the red dots indicate the cones with age dates.

pyroclastic eruptions, often with associated lava flows, and that instead do not clearly follow the general trend of the volcanic arc. The cinder cones of Guatemala and western El Salvador are primarily found behind the stratovolcano trend, in the vicinity of the Ipala Graben (Fig. 2; Williams et al., 1964). The Ipala graben is a roughly N–S trending extensional or transtensional feature produced by the interaction between the strike-slip faults to the north (that form the northern boundary of the Caribbean plate) and with the subduction-zone volcanism to the south (Burkhart and Self, 1985; Carr and Stoiber, 1990; DeMets et al., 1990; Donnelly et al., 1990). The cinder cones in the GSVF are part of a semi-continuous volcanic field with concentrations of cones in the vicinity of the Ipala Graben, Culilapa, Jutiapa and Lago de Güija (Williams et al., 1964; Carr and Stoiber, 1990; Bemis, 1995). The GSVF also includes shield volcanoes, domes and older stratovolcanoes and extends southeastward from Guatemala into El Salvador (Williams et al., 1964; Bemis, 1995). Fig. 2 shows the distribution of cinder cones included in the population studies in this paper.

2.1. Morphology of GSVF cinder cones

The GSVF cinder cones range greatly in size, shape and apparent age. Fig. 3 shows a visual summary of the morphology of these cones. The most notable feature of the GSVF cinder cones is the wide range of angles of slope observed. In fact, the median angle of slope (24°) is well below the so-called pristine angle of slope (33°). There are also a significant number of cones whose morphologic angle of slope is greater than the expected angle of repose. Field observations of nine of the reported cinder cones (Bemis, 1995) found little evidence for agglutination: welded bombs were found at two sites and a scoraceous flow at another but scoria was very to moderately angular at all sites and all nine cones observed in the field are cinder cones not spatter cones. The issue of agglutination will be revisited later.

The mean cone height is $110 +/- 50$ m with a range of 20–270 m. The mean cone basal diameter is $660 +/- 230$ m with a range of 253–1400 m. The average angle of slope is $24° +/- 7°$, the average height-to-radius ratio is $0.33 +/- 0.09$, and the average flatness is $0.24 +/- 0.18$. (A table of the morphologic data is included online as a supplementary electronic file.) The relatively large standard deviations indicate that this population of cinder cones shows significant variability. The bulk of the population of cinder cones in GSVF cluster tightly around the trend $h = 0.33r$ (Fig. 3), with the largest deviations in the larger cones.

2.2. Impact of measurement errors on morphology data

The variance of the angle of slope and the height-to-radius ratio is similar to the maximum errors in these measures, suggesting that much of the variance can be explained by the errors in measuring height, basal diameter, and top diameter. However, a closer inspection of the relationship between primary measurement error and secondary error in calculated morphometric parameters shows that the greatest error is in the smallest cones, which is not surprising because the primary measurement errors are independent of size. Fig. 4 shows the relationship between estimated error and cone size for angle of slope, height-to-radius ratio and flatness. Errors are very high for small cones, so deviations from average or pristine values should be ignored for small cones. The variations in morphology of large cones, however, are reliable and, in general, larger (Fig. 3). As already noted, the bulk of the population of cinder cones in GSVF cluster tightly around the trend $h = 0.33r$ (Fig. 3), with the largest deviations in the larger cones. The steepest and shallowest cones both have basal diameters greater than 600 m. So the variance in angle of slope is not due to measurement error.

2.3. Ages of GSVF cinder cones

Next we look at the dated cones to determine how much of the variance in morphology (especially angle of slope) is due to erosion or degradation over time. Approximately 22 cinder cones in Guatemala and northern El Salvador (GSVF) have been recently dated. Most of these dates are presented in Walker et al. (2011); three are new to this study. All dates utilized are $^{40}Ar/^{39}Ar$ plateau ages. Table 2 lists the new dates. The new dates were measured using step heating, with 11–12 steps at wattages reported in Table 2.

2.4. Morphology over time in GSVF

The morphology of the cinder cones is compared with their age (Fig. 5) to assess the effects of degradation over time. In GSVF, there is no discernable change in morphology over the first million years (no older cones have yet been dated). This suggests whatever erosion and degradation that did occur has not changed the morphology significantly; at least not after the first 50–100 ka, since none of the GSVF cinder cones dated is much younger than 50 ka. Furthermore, the angles of slope of most of the cones are not much different than the pristine value reported in studies of recent or historical cones (Porter, 1972; Wood, 1980a; Hooper and Sheridan, 1998). The surprising finding that the angle of slope does not decrease with age will be discussed later in the context of other regions with dated cinder cones.

3. Comparison of several cinder cone populations

The classic pristine cinder cone has been considered to have an angle of slope of around 33°, a height-to-radius ratio of 0.36 (note the value given in most previous studies uses the diameter so it is half this value), and a flatness of 0.40 (as reported in Wood, 1980a). A detailed review of the
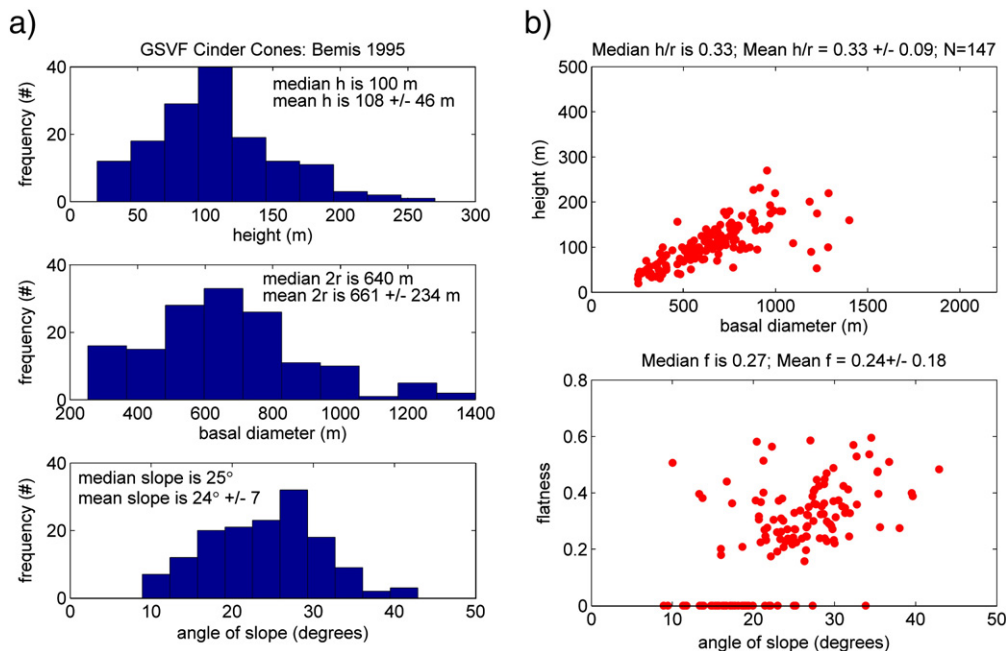

Fig. 3. Summary of cinder cone morphology in GSVF: (a) the population size and angle of slope distributions are more or less normal distributions so we report both population median (for comparison with previous studies) and population mean. (b) The classic comparison of height and diameter is joined by a new morphology plot comparing angle of slope with flatness (the ratio of top – or crater – diameter with basal diameter). Note that wide range in both flatness and angle of slope (despite the narrower range in height-to-radius ratio).
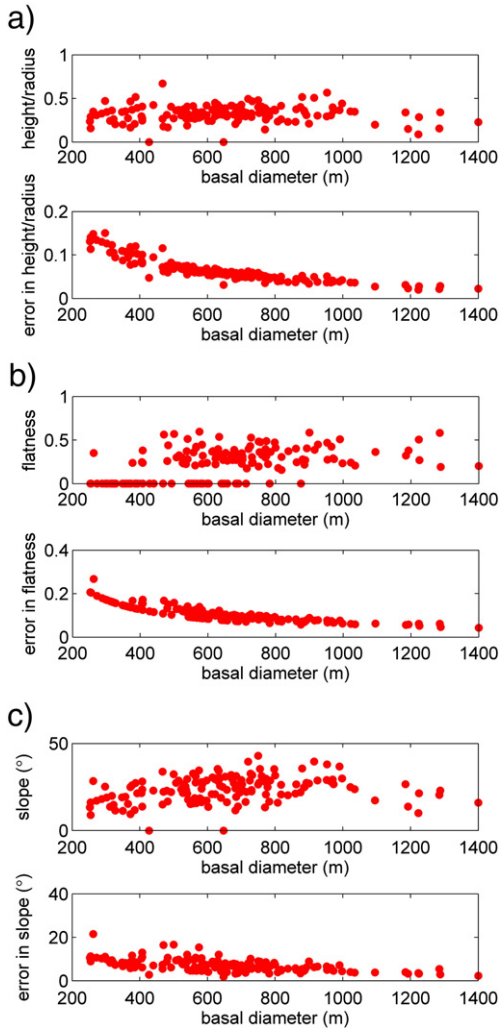
a)

b)

c)

Fig. 4. The change in morphology with size is illustrated by plotting three different calculated measures against basal diameter: (a) height-to-radius ratio, (b) flatness, and (c) angle of slope. Little change with size is observed in the measures themselves, except that angle of slope initially seems to increase and then seems to decrease. The errors, on the other hand, are highly size dependent: the larger (>600 m wide) cones are well-defined but the smaller cones (<400 m wide) may not be.

literature suggests a slightly more complicated picture: Porter (1972) reported a mean angle of slope of 26.5° for cinder cones on the flanks of Mauna Kea, mentioned rare occurrences of much steeper (30°–36°) angles of slope in association with spatter or glaciations, and suggested that the angle of repose was approximately 26°. Bloomfield (1975) reports cinder cones in the Central Mexican Volcanic belt with angles of slope typically 20° to 26°, occasionally reaching 35°, with little correlation to degradational stage. Hooper and Sheridan (1998) report mean average angle of slope as 26° +/− 7° for relatively young cinder cones in the San Francisco Volcanic Field (SFVF). At Mount Etna volcano, the mean slope of 134 parasitic scoria cones is 24°, even if the 72 youngest of them have a mean slope of 25°–26° (see electronic supplement in Favalli et al., 2009). These angles of slope are similar to the average and range of slopes for GSVF cinder cones. However, the accuracy of angle of slope measurements is questionable and angles of slopes are not always reported. It is unclear whether the range of 20° to 36° is just a normal variation in the angle of slope with cone growth, an actual variation in the angle of repose of scoria or, in part, variation due to erosional processes.

Reports of the height-to-radius ratio present a clearer picture. In Porter (1972), the cinder cones lie close to the mean height-to-radius ratio of 0.36. In Bloomfield (1975), the height-to-radius ratio is in the range of 0.38 to 0.42. Wood (1980b) regresses height and diameter to yield a typical

height-to-radius ratio of 0.36 for young cones in the SFVF. Hooper and Sheridan (1998) also find a height-to-radius ratio of 0.36 for cones in the SFVF. Settle (1979) suggests that a height-to-radius ratio of 0.40 fits the cinder cone populations of Mauna Kea and of Mt Etna, although he also reports other volcanic fields with lower height-to-radius ratios. Recently, Favalli et al. (2009) estimated the average height-to-radius ratio for cinder cones on Mt Etna as closer to 0.38, indicating that heights must be estimated based on net elevation differences of original base to top on sloped surfaces. The GSVF cones of this study have a mean height-to-radius ratio of 0.33, somewhat lower than previous studies, but well within the estimated error (0.05).

Flatness (the ratio of top diameter – or crater width – to basal diameter) has also been suggested to be relatively constant for young cones. Porter (1972) suggests a typical flatness of 0.40 for cinder cones on Mauna Kea. Bloomfield (1975) also reports an average flatness of 0.40 for young cones in the central Mexican Volcanic Belt with flatness increasing substantially in older cones (up to 0.83). In contrast, Wood (1980b) finds that flatness doesn't change much in older cones of the SFVF from the typical value of 0.40 for young cones in both the SFVF and worldwide. The GSVF cinder cones of this study have an average flatness of 0.24 but a range of flatness from very small (flatness<0.06 is undistinguishable from zero) up to 0.60, although other small volcanoes in GSVF identified as maars have even higher flatnesses. The biggest difference from the reported data for young cones is the very large range of values for flatness in the GSVF cones.

Most of the published studies of cinder cones cited above report only incomplete and summary information on cinder cones. Some of the studies look at a single geologically defined population and some compare young cones worldwide. It is often difficult to discern if other populations of cinder cones show similar variability to those in GSVF; furthermore, it is important to see if there is a difference in how populations change with age. A few studies of other populations of cinder cones have published the actual cone parameters and, in some cases, cone ages (Hasenaka and Carmichael, 1985a, 1985b; Dohrenwend et al., 1986; Wood, 1979; Carn, 2000). We compare the GSVF cones with these published populations to see what features are typical and what are not; also we wish to discern the source of the variations in the angle of slope and flatness. The key populations in this comparison are from the San Francisco volcanic field in Arizona, the Cima volcanic field in California, the Michoácan–Guanajuato volcanic field in Mexico, and the Lamongan volcanic field in Java.

The San Francisco volcanic field (SFVF) has been extensively studied: first by Settle (1979) and Wood (1979, 1980a, 1980b) and later by Hooper (1994) and Hooper and Sheridan (1998). Sited on the edge of the Colorado Plateau, volcanism began in the western part of the field around 6 Ma and has shifted eastward over time; the youngest cone erupted about 900 a. The SFVF population of cinder cones used here includes cones of all ages. Morphology measurements were made from 1:24,000 or 1:50,000 topographic maps with contour intervals of 10–20 m.

The Cima volcanic field occurs in the arid environment of the eastern Mohave Desert. Two pulses of volcanism have occurred in the Cima volcanic field. The first volcanic activity occurred from ~3 to 5 Ma and the second pulse of volcanic active occurred form ~1.0 to 0.1 (Turrin et al., 1984; 1985). Dohrenwend et al. (1986) studied the morphology of 11 of 31 cones. The study explicitly excluded cinder cones with complex structures (tepha rings or overlapping craters) as well as undated cones. Morphology measurements were made primarily in the field or from aerial photographs but calibrated to 1:24,000 scale topographic maps with a contour interval of 10 m.

The Lamongan volcanic field in East Java, Indonesia lies along the Sunda volcanic arc on the flanks of the Lamongan volcano, which has had several basaltic lava effusive events in recent history (Carn, 2000). The volcanic field includes 61 cinder or spatter cones, at least 29 maars and the main volcanic complex. Carn (2000) reports morphologic data for 22 maars and 36 cinder or spatter cones. No age dates

Table 2
New ^{40}Ar/^{39}Ar dates.[a] Summary of ages (boldface indicates sample data for ages used in this study).

Volcano name	Sample	ID	Irrad.	Material	Inter age	Error	% rad	Age	± 1s	MSWD	Prob.	Steps	n/n-total	Age used
Cerro el Tablon	guc1007s	20255-01	17e	glassy-matrix	896	14	16.3	631	6	2.7	0.05	G–J	4/11	
	guc403	**20260-01**	**17e**	**wr-matrix**	**679**	**12**	**17.7**	**705**	**7**	**1.1**	**0.34**	**B–K**	**10/12**	**705**
Cerro San Jeronimo	guc309	20259-01	17e	wr-matrix	1050	160	2	220	40	0.6	0.69	A–G	7/12	
	guc1003s	**20256-01**	**17e**	**glassy-matrix**	**730**	**40**	**5.4**	**581**	**16**	**0.6**	**0.68**	**F–K**	**6/11**	**581**
Cerro el Reparo	**guc1004s**	**20257-01**	**17e**	**glassy-matrix**	**200**	**20**	**2.7**	**240**	**9**	**3.2**	**0.01**	**D–I**	**6/11**	**240**
	guc709	20258-01	17e	wr-matrix	285	10	8.6	306	8	1.4	0.23	D–H	5/12	

Volcano name	Sample	ID	Age	± 1s	^{40}Ar/^{36}Ar init	± 1s	MSWD	n
Isochron from plateau data								
Cerro el Tablon	guc1007s	20255-01	610	40	298.3	5.7	3.519	4
	guc403	20260-01	726	18	293.1	1.9	1.039	10
Cerro San Jeronimo	guc309	20259-01	420	160	293.7	2	0.604	7
	guc1003s	20256-01	550	80	298	6	0.741	6
Cerro el Reparo	guc1004s	20257-01	280	30	293	1.8	2.758	6
	guc709	20258-01	170	70	310.4	12.9	1.255	5

Run ID	Watts	Ca/K	Cl/K	^{36}Ar/^{39}Ar	%^{36}Ar(Ca)	^{40*}Ar/^{39}Ar	% ^{39}Ar step	Cum. %^{39}Ar	%^{40}Ar*	Age (ka)	± Age
^{40}Ar/^{39}Ar Step-Heating data for runs 20257-01, 20258-01; guc1004s, guc709											
guc1007s, Run ID# 20255-01 (J = 0.00009 ± 1.000000e−6):											
20255-01A	1	−0.98666	0.03115	1.793261	0	10.07774	0.6	0.6	1.9	1635.55088	590.4513
20255-01B	2	1.98504	0.01249	0.833268	0	8.84497	1.9	2.5	3.5	1115.04968	134.74193
20255-01C	4	2.82727	0.00904	0.342816	0.1	8.78946	3.7	6.2	8	1108.05446	62.17972
20255-01D	6	3.43569	0.0035	0.095078	0.5	5.90192	8.5	14.7	17.4	744.10849	19.11943
20255-01E	8	3.87335	0.00405	0.042771	1.3	5.72769	13.8	28.5	31.4	722.14553	11.42873
20255-01F	10	4.41214	0.00559	0.04047	1.5	5.40567	15.8	44.3	31.4	681.55376	10.40996
•20255-01G	12	4.11522	0.00746	0.043676	1.3	5.0838	13.1	57.4	28.5	640.97873	11.40801
•20255-01H	15	4.24842	0.00869	0.047458	1.2	5.03169	17.7	75	26.6	634.40946	9.71475
•20255-01I	20	5.48315	0.00785	0.057442	1.3	4.80074	14.5	89.5	22.2	605.29597	12.1785
•20255-01J	25	6.99629	0.01162	0.121049	0.8	5.37023	5.7	95.2	13.1	677.08519	28.19516
20255-01K	35	7.33987	0.0018	0.162251	0.6	6.05473	4.8	100	11.2	763.36963	34.75676
Integ. age=										896	14
(•) Plateau age =							50.9			631	6
guc403, Run ID# 20260-01 (J = 0.0000699 ± 8.970000e-8):											
20260-01A	1	75.04365	−0.59995	1.281525	0.8	−85.88257	0.1	0.1	−28.6	−10862.86	2650.49605
•20260-01B	2	3.66321	−0.04218	0.7021	0.1	2.3062	0.6	0.7	1.1	290.80002	335.27736
•20260-01C	4	7.18341	−0.01502	0.221927	0.4	5.25447	4.5	5.1	7.4	662.49365	58.82374
•20260-01D	6	3.60565	−0.00449	0.140995	0.4	5.49734	8.3	13.5	11.7	693.10936	34.19054
•20260-01E	8	5.76217	−0.00365	0.098908	0.8	5.48899	11.7	25.2	15.9	692.05641	23.67619
•20260-01F	10	3.70889	−0.00363	0.076698	0.7	5.49114	10.9	36.1	19.6	692.3273	21.81533
•20260-01G	12	3.60048	0.00358	0.063504	0.8	5.69676	8.8	44.9	23.4	718.2471	21.33421
•20260-01H	15	2.53721	0.00002	0.053799	0.7	5.69777	10.4	55.3	26.5	718.37397	19.69696
•20260-01I	20	6.33256	0.00123	0.052615	1.7	5.46846	16.6	71.9	26.3	689.46791	14.84313
•20260-01J	25	9.91586	0.00706	0.058637	2.3	5.55665	12.4	84.3	24.7	700.58578	20.9032
•20260-01K	35	15.00004	0.00444	0.063322	3.3	6.05098	9.6	94	25	762.89693	25.16233
20260-01L	40	11.49661	0.00162	0.082254	1.9	4.86919	6	100	16.9	613.92483	38.10321
Integ. age=										679	12
(•) Plateau age =							93.9			705	7
guc309, Run ID# 20259-01 (J = 0.00009 ± 1.000000e-6):											
•20259-01A	1	0.99165	−0.05087	3.536186	0	−10.44668	0.2	0.2	−1	−1696.9936	1832.51785
•20259-01B	2	−0.34658	0.02702	1.602125	0	−0.65793	1.8	2	−0.1	−106.82987	399.38928
•20259-01C	4	3.28987	0.01997	0.908175	0.1	2.37771	8.9	10.9	0.9	299.8164	96.35377
•20259-01D	6	6.85077	0.00404	0.786844	0.1	2.11058	10.8	21.7	0.9	266.13535	77.24564
•20259-01E	8	9.39746	−0.01123	0.745397	0.2	1.13582	12.6	34.3	0.5	143.22679	135.63071
•20259-01F	10	6.88365	0.00156	0.762195	0.1	1.00318	12.9	47.2	0.4	126.50112	113.88278
•20259-01G	12	7.26788	0.00524	0.91152	0.1	1.55969	11.8	58.9	0.6	196.67383	90.89204
20259-01H	15	−0.73519	0.01796	1.142175	0	15.53362	12.6	71.5	4.4	1957.80458	202.57219
20259-01I	20	5.6792	0.01177	1.466607	0.1	16.70979	12.9	84.4	3.7	2105.95839	642.47828
20259-01J	25	8.70277	0.02625	1.796238	0.1	11.53429	8	92.4	2.1	1453.94546	224.82218
20259-01K	35	10.00822	0.03217	1.256524	0.1	7.42396	5.1	97.5	2	935.95619	182.37364
20259-01L	40	7.99982	0.02926	1.148504	0.1	10.50322	2.5	100	3	1324.02296	263.45448
Integ. age=										1050	160
(•) Plateau age =							58.9			220	40
guc1003s, Run ID# 20256-01 (J = 0.00009 ± 1.000000e−6):											
20256-01A	1	−7.99109	−0.05012	5.796754	0	−3.5372	0.7	0.7	−0.2	−574.41645	1345.42228
20256-01B	2	3.81473	0.00049	3.472008	0	9.5506	1.7	2.5	0.9	1550.03565	764.97513
20256-01C	4	5.05666	0.01462	1.083179	0.1	2.11276	4	6.5	0.7	266.41051	187.42774
20256-01D	6	5.54884	0.03917	0.281626	0.3	5.86135	8.1	14.6	6.6	738.99369	97.07554
20256-01E	8	5.68791	0.0191	0.126593	0.6	3.72906	15	29.6	9.1	470.19149	34.09658
•20256-01F	10	6.64206	0.02267	0.098167	0.9	4.81865	16.7	46.3	14.3	607.55313	30.73879
•20256-01G	12	8.06909	0.02468	0.093313	1.2	4.72836	14.9	61.2	14.8	596.17099	31.9516
•20256-01H	15	7.67656	0.02844	0.091707	1.2	4.36941	17.9	79.1	14	550.91991	28.97288
•20256-01I	20	7.38796	0.02827	0.120087	0.9	4.41308	13.4	92.4	11.1	556.4255	37.74461
•20256-01J	25	8.44171	0.02043	0.177078	0.7	5.31857	3.9	96.4	9.3	670.57323	109.44595
•20256-01K	35	9.64399	0.01231	0.210715	0.6	4.71516	3.6	100	7.1	594.50775	118.045
Integ. age=										730	40
(•) Plateau age =							70.4			581	16

Table 2 (continued)

Run ID	Watts	Ca/K	Cl/K	^{36}Ar/^{39}Ar	%^{36}Ar(Ca)	^{40*}Ar/^{39}Ar	% ^{39}Ar step	Cum. %^{39}Ar	%^{40}Ar*	Age (ka)	± Age
guc1004s, Run ID# 20257-01 (J = 0.0000699 ± 8.970000e−8):											
20257-01A	1	−0.48845	−0.10682	0.950441	0	−9.56876	0.7	0.7	−3.5	−1207.0726	362.13333
20257-01B	2	0.25651	−0.02149	0.670075	0	−0.58635	2	2.7	−0.3	−73.94375	144.24338
20257-01C	4	3.294	0.00637	0.704145	0.1	−4.0538	5.2	7.9	−2	−511.27652	200.36105
•20257-01D	6	3.96483	0.01759	0.352698	0.2	1.35422	10.3	18.2	1.3	170.76551	40.27077
•20257-01E	8	4.50609	0.01205	0.181255	0.3	1.53783	13.4	31.6	2.8	193.91819	23.27822
•20257-01F	10	5.34423	0.01573	0.144127	0.5	2.03431	14.2	45.8	4.6	256.51856	21.98543
•20257-01G	12	5.9516	0.01152	0.106855	0.8	2.15796	12.9	58.7	6.4	272.10853	22.0618
•20257-01H	15	5.84272	0.00869	0.085107	1	1.66453	15.3	74	6.3	209.89388	18.20967
•20257-01I	20	5.61329	0.01335	0.082306	0.9	2.1765	15.5	89.5	8.3	274.4467	17.36444
20257-01J	25	5.41943	0.00975	0.104543	0.7	3.9421	5.6	95.1	11.4	497.04951	45.20692
20257-01K	35	7.77185	0.01309	0.133237	0.8	2.78497	4.9	100	6.6	351.16494	44.11251
Integ. age=										200	20
(•) Plateau age =						81.6				240	9
guc709, Run ID# 20258-01 (J = 0.0000699 ± 8.970000e−8):											
20258-01A	1	27.57915	0.07154	0.301708	1.3	−1.9818	0.2	0.2	−2.3	−249.93221	664.62772
20258-01B	2	−0.63526	0.00619	0.18009	0	3.60874	1.6	1.9	6.3	455.02264	108.60649
20258-01C	4	2.53447	0.0171	0.121258	0.3	1.64153	7.6	9.5	4.4	206.99339	26.50038
•20258-01D	6	2.60064	0.00902	0.083167	0.4	2.60493	11.1	20.5	9.6	328.46509	19.90864
•20258-01E	8	4.00579	0.00903	0.070965	0.8	2.35941	13.7	34.2	10.2	297.50875	16.26897
•20258-01F	10	5.42479	0.00747	0.067806	1.1	2.25011	14.5	48.7	10.2	283.72796	15.51928
•20258-01G	12	4.50539	0.01266	0.066299	0.9	2.40801	12.7	61.5	11	303.63652	16.31012
•20258-01H	15	4.71216	0.00529	0.068962	0.9	2.63371	12.2	73.7	11.5	332.09339	18.41195
20258-01I	20	7.04368	0.01153	0.07821	1.2	2.85678	11.8	85.5	11.1	360.21826	18.18497
20258-01J	25	6.80735	0.01367	0.097788	1	1.89849	7.6	93.1	6.2	239.39325	27.44634
20258-01K	35	4.02875	0.00835	0.087557	0.6	1.27792	3.7	96.8	4.7	161.14511	53.05257
20258-01L	40	5.04395	0.01015	0.093205	0.8	0.81651	3.2	100	2.9	102.96356	60.29344
Integ. age=										285	10
(•) Plateau age =						64.2				306	8

[a] The ^{40}Ar/^{39}Ar measurements were done at the recently constructed ^{40}Ar/^{39}Ar dating lab at Rutgers University using methods similar to those of Turrin et al. (1994, 1998).

are reported although the maars are mostly Pleistocene and the cinder cones more recent. Morphology measurements made either from 1:50,000 scale topographic maps, a SPOT satellite image, geologic maps or field work; no information on contour interval reported. No distinction between cinder and spatter cones was made in the reported morphology data.

The Michoácan–Guanajuato volcanic field (MGVF) in central Mexico lies within the Mexican Volcanic Belt, which is related to the subduction of the Cocos Plate. The volcanic field contains a variety of types of volcanoes,

including 901 cones, 43 domes, 13 shield volcanoes, and 22 maars. The historical eruptions of the cinder cones Paricutin and Jorullo occurred in this volcanic field. Hasenaka and Carmichael (1985a) report morphologic and age data for 11 cinder cones. Morphology measurements were made from 1:50,000 topographic maps with contour intervals of usually 20 m (sometimes 10 m).

Table 3 lists mean values for the morphologic parameters considered in this study. In a broad sense, the GSVF cinder cones are similar to cinder cones in the other volcanic fields. However, each field
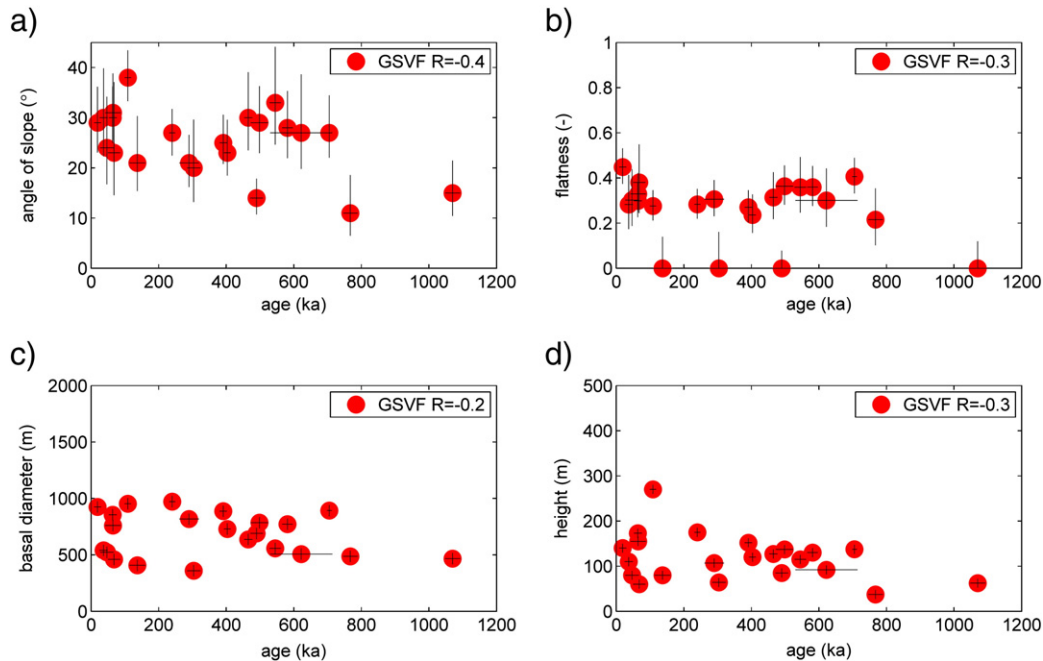

Fig. 5. Various morphological parameters are plotted against cone age for cinder cones in GSVF: (a) angle of slope. (b) Flatness. (c) Basal diameter. (d) Height. None of them change systematically with age. In particular, the angle of slope does not systematically decrease with age, although the very lowest angles of slope are all in older cinder cones.

Table 3
Population morphology and comparison.

Morphologic measures for several populations of cinder cones

Population	N	Height	Basal Diameter	Top Diameter	h/r	Angle of slope	Flatness
GSVF*	147	110 +/- 50	672 +/- 236	181 +/- 146	0.33 +/- 0.09	24° +/- 7°	0.24 +/- 0.17
Cima, USA	11	95 +/- 29	597 +/- 138	185 +/- 113	0.32 +/- 0.05	25° +/- 6°	0.30 +/- 0.17
Lamongan, Java	22	94 +/- 57	747 +/- 444	30 +/- 43	0.26 +/- 0.07	24° +/- 8°	0.08 +/- 0.11
MGVF, Mexico	11	170 +/- 68	955 +/- 243	308 +/- 126	0.35 +/- 0.11	27° +/- 8°	0.32 +/- 0.08
SFVF	67	136 +/- 85	1093+/- 491	152 +/- 216	0.24 +/- 0.09	16° +/- 7°	0.14 +/- 0.19
Classic pristine	---	---	----	----	0.36	25° - 33°	0.40

Statistical comparisons of populations based on student's t-test distribution and sample means above

	Cima	Lamongan	MGVF	SFVF
GSVF*	**Slope: df=166, t= -0.45, p=0.65** **Flatness: df=166, t= -1.06, p=0.29**	**Slope: df=191, t=0.07, p=0.94** Flatness: df=191, t=5.46, p=1.5×10^{-7}	**Slope: df=166, t= -1.25, p=0.21** **Flatness: df=166, t= -1.40, p=0.16**	Slope: df=222, t=7.38, p=3.1×10^{-12} Flatness: df=222, t=3.69, p=2.9×10^{-4}
Cima		**Slope: df=45, t= -0.43, p=0.67** Flatness: df=45, t= -5.03, p=8.2×10^{-6}	**Slope: df=20, t= -0.63, p=0.54** **Flatness: df=20, t= -0.30, p=0.77**	Slope: df=76, t=4.00, p=1.5×10^{-4} **Flatness: df=76, t=1.87, p=0.065**
Lamongan			**Slope: df=45, t= -1.08, p=0.29** Flatness: df=45, t= -6.48, p=6.1×10^{-8}	Slope: df=101, t=5.07, p=1.8×10^{-6} Flatness: df=101, t= -2.02, p=0.046
MGVF				Slope: df=76, t=4.65, p=1.4×10^{-5} Flatness: df=76, t=2.92, p=4.6×10^{-3}

The terms reported above are defined as follows: df = degrees of freedom; t = value of t-test statistic; p = probability of t-test statistic occurring coincidentally. All values are calculated using Matlab's t-test function. Values of p > 0.05 indicate that the two sampled populations compared could come from the same ideal population distribution function (indicated by boldface table entries).

shows a distinct character. The Lamongan cinder cones have very low flatness, due to very small craters relative to the size of the cone. The SFVF cinder cone population has a low mean angle of slope and low mean flatness, possibly because it includes more older cones. The MGVF cones have higher height-to-radius ratios (but not higher angles of slope) and high flatness.

In comparing the GSVF cones with the populations of cones from other areas, the most noticeable feature is the larger number (147) of GSVF cones (Fig. 6a). This mostly reflects the comprehensiveness of the GSVF study (Bemis, 1995) which attempted to locate, classify and characterize every volcano in Guatemala and western El Salvador (from Santa Maria to San Salvador; see Fig. 2 for study extent). Wood's (1979) study comes closest to matching the GSVF study in scope, but the region covered is smaller.

Broadly speaking, most of the cones, in the combined set of volcanic fields, cluster around a height-to-radius ratio of 0.36 (Fig. 6c). The generally lower population means for height-to-radius ratio reflect that most of the deviating cones fall below the "pristine" line on Fig. 6a (that is, they have a lower height-to-radius ratio). If the mean and standard deviation of the GSVF population are used to define a "pristine" cone region, the GSVF, Cima, and MGVF cones all fall within that region. Most of the SFVF and Java cones do not.

Looking at a flatness versus angle of slope plot (Fig. 6b), the GSVF cinder cones cover a larger morphologic space than any other single volcanic field's cinder cone population. Some of this may be due to the comprehensive coverage of the population, but the SFVF similarly approaches 100% coverage and the other data sets have ~30% coverage. So we would expect the ranges to be closer.

The mean GSVF, MGVF, and Cima cinder cones come close to matching the classic "pristine" cone, except for lower flatness (Fig. 6d and e; Table 3). However, the populations cover a broad range of values. Inspection of Fig. 6 (and actual statistical comparisons of populations reported in Table 3) suggests that the sampled cones of GSVF, MGVF, and Cima could have come from the same ideal

population, but that the Lamongan and SFVF cones must be from a different ideal population, despite the overlap of population standard deviations. Another recent study also found considerable variation in cone morpholgy (Kervyn et al., 2010).

Overall, the combined population of cinder cones has a broad range of slopes between 10 and 35°. The angle of slope is controlled by the angle of repose of scoria, which is probably similar between regions but may vary slightly with grain size. So a modest range of angles of slope would be expected (slightly lower where grains are smaller and slightly higher where grains are larger assuming angularity accounts for most of the variation in angle of repose and vesicularity for most of the variation in angularity). The observed slopes may vary more than anticipated, whether due to erosion, early cessation of constructing eruptions, or variations in angle of repose. The affects of constructional processes will be discussed later.

Flatness seems to vary even more between populations than the angle of slope (Fig. 6 b, d, and e). It is not apparent what controls flatness, but, since in most cases the top diameter is the crater diameter, it seems likely to be related to the explosivity or the width of the explosive conduit. It is possible that the variable presence of meteoric water (or groundwater) would result in a variable increase in explosivity and thus crater width. It is interesting that in GSVF, the cinder cones and maars appear to form a continuum of morphologies; however, this may be a coincidence because the maars can be distinguished from the cinder cones based on the depth and distinctly expressed crater morphology. In contrast, the maars present in the Lamongan volcanic field are significantly larger in diameter than the cinder cones.

Fig. 7 considers the dated cones in four of the above populations. There are not very many dates in any region (22 dates in GSVF; 11 in Cima; 11 in MGVF; and 17 in SFVF). Noticeably, only the Dohrenwend et al. (1986) data set for Cima shows any consistent variation in morphology with age. For Cima, the angles of slope noticeable decrease with age and the flatness may also decrease with age. On the
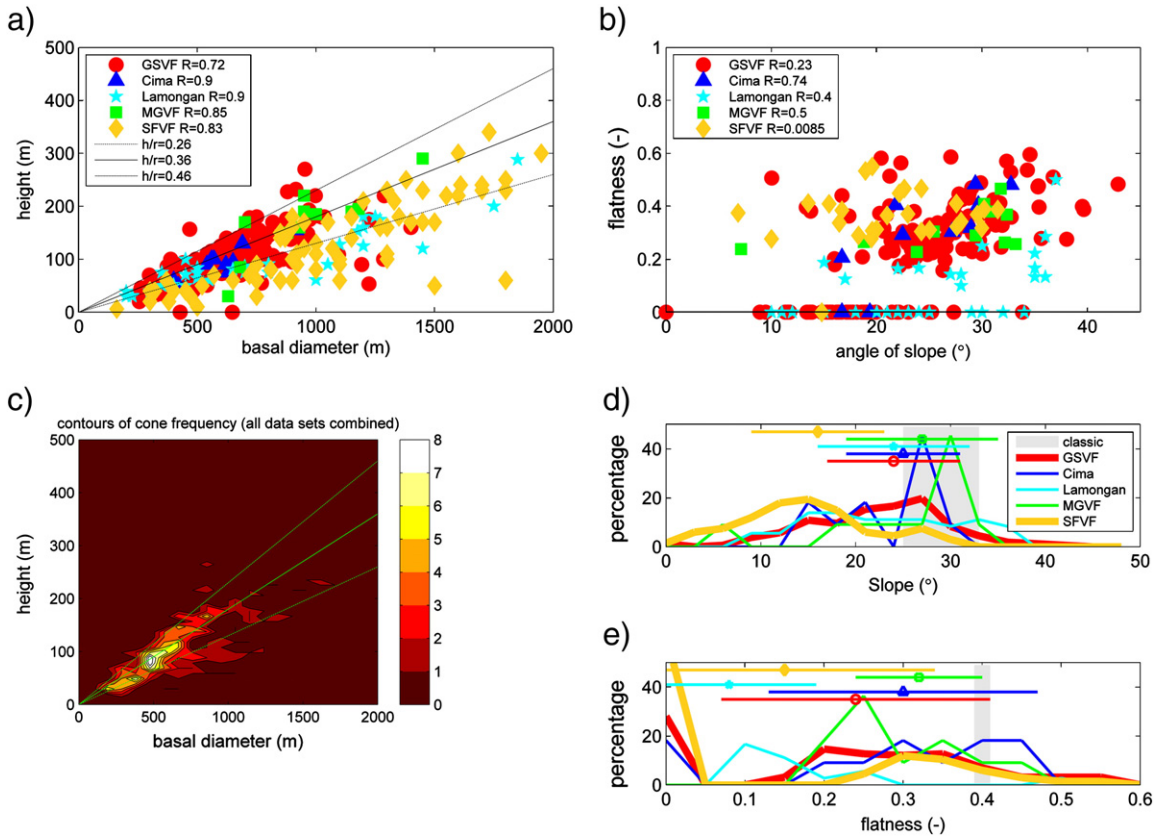
Fig. 6. Plotting multiple populations on the same graph gives an immediate sense of their differences. (a) The GSVF, MGVF, and Cima cones are clustered around the height-to-radius line for pristine cones. The gray lines show the mean height-to-radius radio of 0.36 for the GSVF cones (solid line) and the standard deviations on each side (dotted lines). Many of Wood's (1979) cones in the San Francisco Volcanic Field are outside this range — notably these are the older cones, which he identifies as partially eroded. The correlation coefficients between height and basal diameter are reported in the figure legend for each population. (b) The ranges of angles of slope and flatnesses are similar for all the regions, except the Lamongan cones have only flatnesses on the lower end of the range of the others. (c) The combined populations are contoured on the height versus basal diameter graph to show that the majority of cones cluster around a height-to-radius ratio of 0.36 (solid green line). (d) The probability distribution functions (curves) for slope for the different populations are shown along with the mean (symbols) and standard deviations (straight lines). (e) The probability distribution functions (curves) for flatness for the different populations are shown along with the mean (symbols) and standard deviations (straight lines). Note that the mean is not always a very good summary of the population.
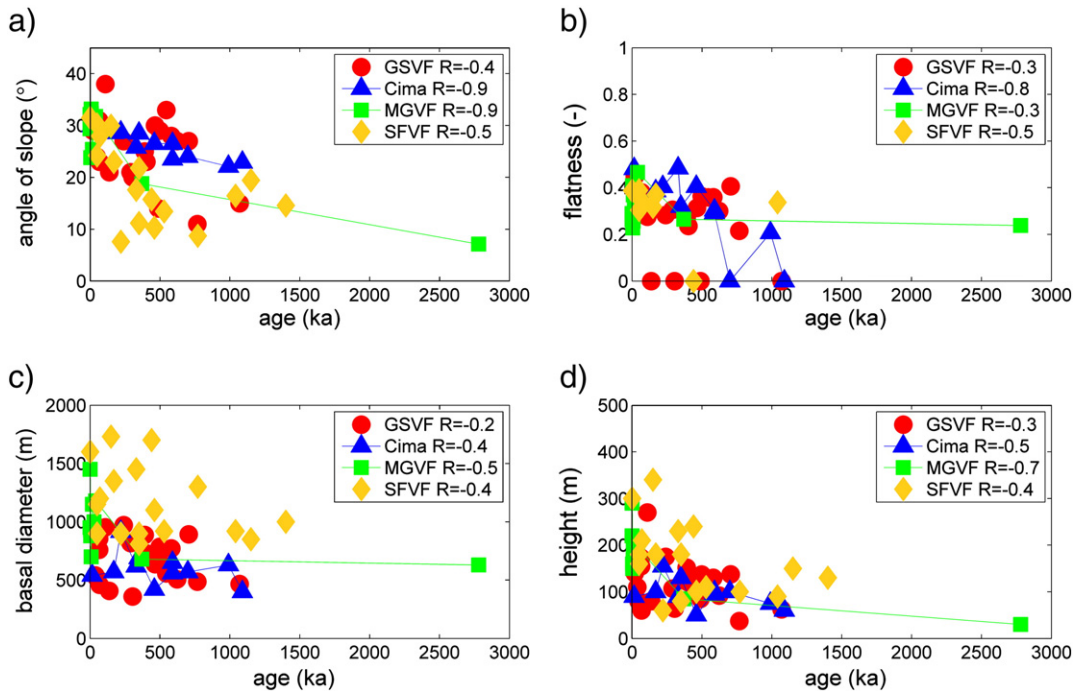
Fig. 7. The morphologic measures angle of slope (a), flatness (b), basal diameter (c) and height (d) are plotted against age for the cinder cones of GSVF, Cima, MGVF and SFVF.
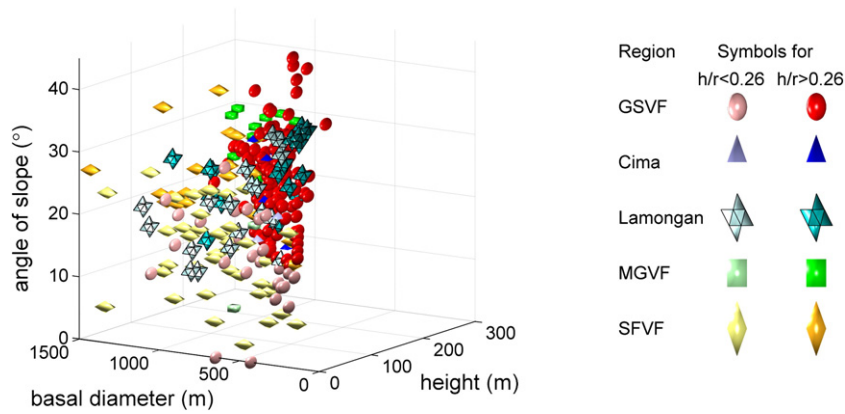
Fig. 8. Making a distinction those cones that have high h/r (black dots) and those with low h/r (white dots) suggests that some cones with low angles of slope ceased erupting while still in the early growth phase while other cones with low angles of slope have broad bases that may have been created by erosion.

other hand, the Cima population has the least variation in cone size (height or basal diameter) and cone shape (angle of slope or flatness). Dohrenwend et al. (1986) also used detailed surveying methods to quantify the geomorphic features used to classify cones, including such geomorphic features as gully number and dimension. As mentioned above, in addition to the arid environmental conditions, the study explicitly excluded cinder cones with complex structures. The Bemis (1995) study of the GSVF cones showed no significant correlation between morphology and geomorphic indicators of erosional stages.

The SFVF also has generally decreasing angles of slope with age, but only for the younger (<500 ka) cones. In contrast, there is no evidence in GSVF of any significant decrease in angles of slope over the first 1000 ka. Less can be said about MGVF, where the data available to this study only included two older cones. In contrast to predictions of models of cinder cone degradation (Wood, 1980b; Dohrenwend et al., 1986; Hooper and Sheridan, 1998), no region shows any significant variation in basal diameter with age.

4. Models of growth and erosion

Conceptually, cinder cones grow first by increasing in height and angle of slope, then by increasing jointly in height and basal diameter (McGetchin et al., 1974). If a population of cinder cones represents multiple stages of growth, smaller cones would show a correlation between angle of slope and height and larger cones a correlation between height and basal diameter. The correlation between height and basal diameter would also be found in a population representing variable

volumes or fluxes of magma but with each cone reaching the final stage of growth (where the early stage of growth would be undetectable). This says little about the relationship of flatness to growth.

The populations discussed in this paper all show strong correlations between height and basal diameter (see legend of Fig. 6 for correlation values). Furthermore, most of the cones are within one standard deviation of the mean or pristine height-to-radius ratio. Given the relatively large measurements errors (inevitable on the 1:50,000 scale maps most of the studies used), most cones are following the expectations of both growth models and earlier studies of cone growth. The main exceptions are the older cones in SFVF and the larger cones from Lamongan. Some cones in GSVF fall outside the "pristine" range on both sides, in contrast with the cones of SFVF and Lamongan which lie on the lower height-to-radius side of the range only.

Of course, real populations are also affected by erosion and degradation and by the mutual impact of multiple volcanic eruptions (i.e. later lava flows or ash falls can disguise or alter the cone morphology). Studies of cinder cone erosion suggest that, during erosion, material is transferred from the top of the cone to a sediment apron around the base of the cone (Dohrenwend et al., 1986; Hooper and Sheridan, 1998). Thus as cones got older, they would get shorter heights, wider bases and gentler slopes. Assuming the cones within a volcanic field erupted over time and have different ages, this would predict a reduction in height-to-radius ratio over time and in angle of slope over time as well as a negative correlation between angle of slope and basal diameter.

Unfortunately for this conceptual model, not all volcanic fields show much change in cone morphology with cone age (Fig. 7). The Cima and San Francisco volcanic fields do show a strong initial
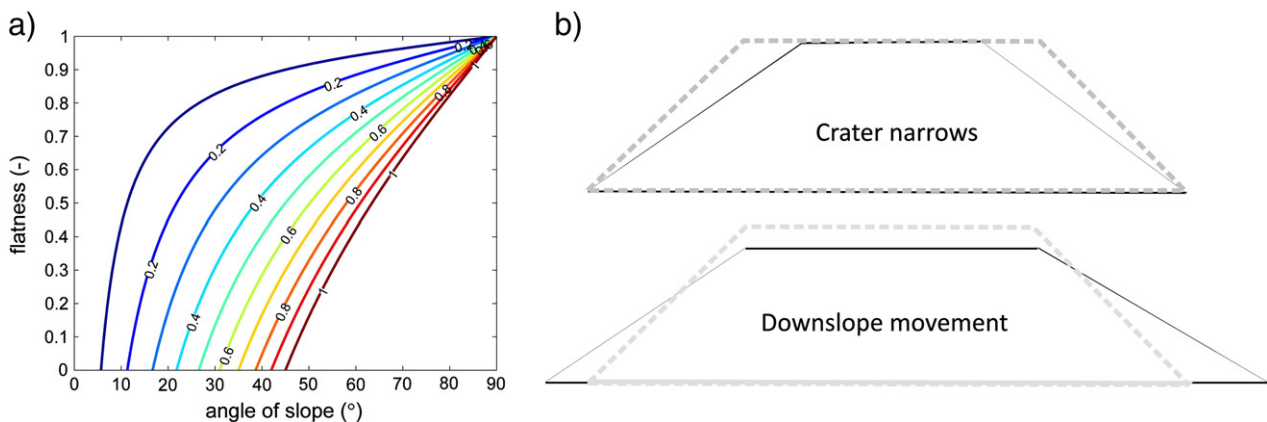

Fig. 9. (a) Contours of height-to-radius ratio are presented on a plot of flatness versus angle of slope. The main point is a line of constant height-to-radius ratio is a line of variable flatness and angle of slope while a line of constant flatness is a line of variable angle of slope and height-to-radius ratio. (b) An illustration of how changing flatness changes angle of slope. The dashed cone outline is exactly the same in both examples.
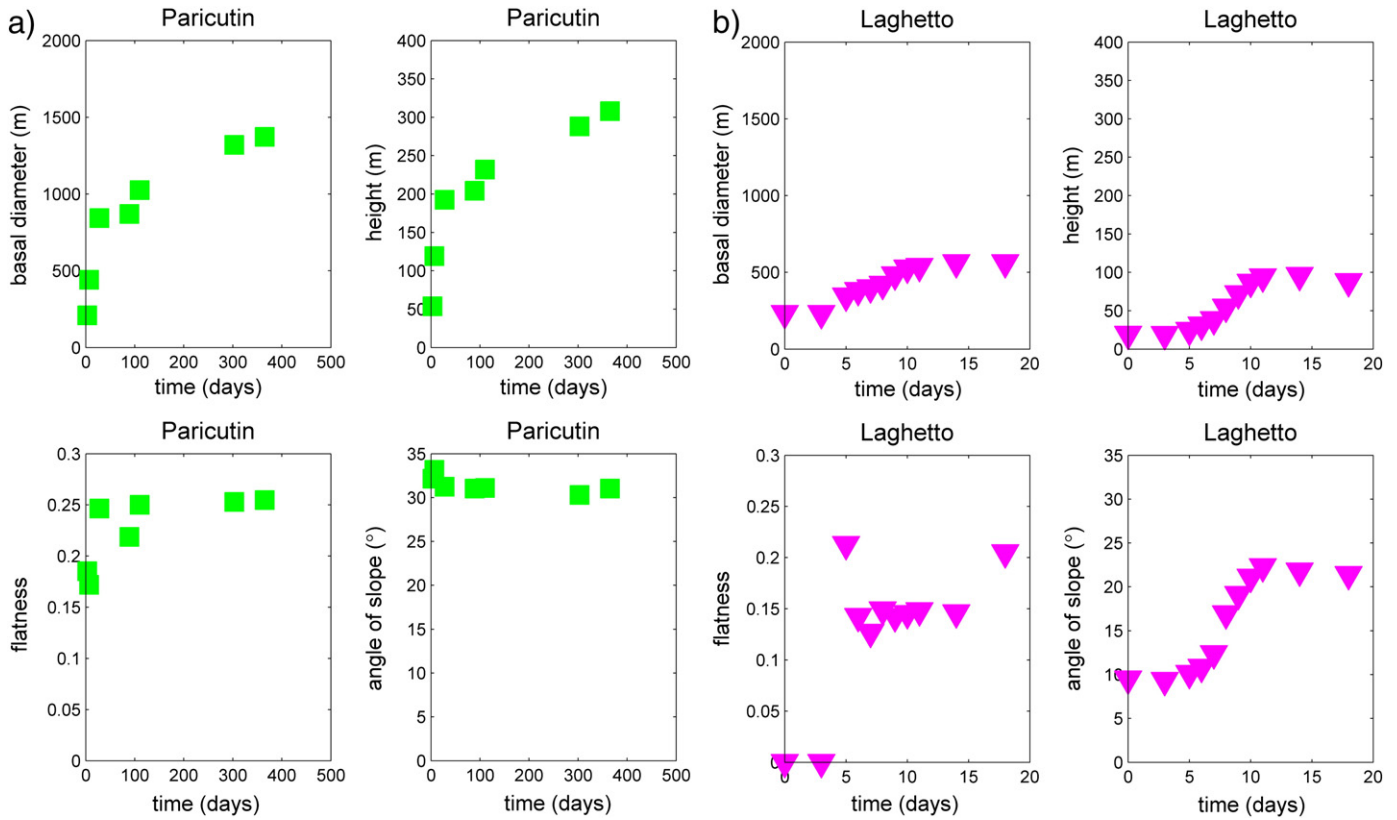
Fig. 10. The growth patterns of Paricutin (a) and Laghetto (b) are shown as plots against time for cone diameter, cone height, flatness and angle of slope. Paricutin is much larger than Laghetto; nevertheless, they both increase quickly in height and basal diameter with generally constant (although different) flatness. Laghetto gets off to a slow start (observers note the eruption began with a phreatomagmatic phase). Once it starts growing, Laghetto increases rapidly but visibly in angle of slope. Here we actually can see the early growth phase of a cinder cone. The angles of slope shown here are average angles of slope for the entire profiles. Average angles of slope are often significantly lower than the maximum angles of slope, especially if the angle of slope near the rim is steeper than at the base of the cone (Laghetto has a shallow apron surrounding a steeper center for most of the later stages).

decrease in angle of slope as the cones get older up to about 500 ka, after which the angle of slope of the cones in the SFVF remains within a constant range. The GSVF cones show no change in angle of slope with cone age. One explanation is the difference in climate: both Cima and SFVF are in relatively arid climates where there is limited vegetation covering the cones. The GSVF cones are in a more tropical climate with rapid soil development (quarried cones generally show at least a meter of soil on top of the scoria) and rapid growth of grass and trees. The vegetation may limit the extent of degradation, preserving the overall cone morphology longer.

Another issue is the affect of agglutination or spatter on the way a cinder cone erodes: significant spatter on the crater rim could reduce erosion of the rim, which might lead to steeper angles of slope with age or more variable angles of slope with age. While there is insufficient field evidence to rule out the possible affect of spatter, there is also no evidence for any systematic effects. None of the areas show increasing angles of slope or variability in angles of slope with age.

So the paradox of the data presented here is: the GSVF cinder cones show little variation in cone morphology with age but the largest overall variability in morphology. If erosion doesn't create the variation in morphology, something else must. We suggest the variance in morphology is largely primary: growing cones increase

in angle of slope at least until the angle of repose is reached. We agree that pristine (uneroded) cones usually have higher height-to-radius ratios and use that to distinguish two types of cones with low angles of slope: (1) those that also have both low height and low basal diameter and (2) those that have higher basal diameters especially relative to their heights. Fig. 8 shows that most of the GSVF cones fall in type 1, which we interpret as relatively uneroded cones that ceased erupting without achieving its maximum steepness. In contrast, most of the cones in the SFVF fall into type 2, which we interpret as eroded cones. Cima, surprisingly, follows the GSVF trend. The trend of the Lamongan cones cuts across the other trends.

Part of what is happening in Cima can be explained by referring back to the flatness versus angle of slope plot (Fig. 6b). The change in angle of slope in the Cima cones is correlated with a change in flatness; furthermore, both flatness and angle of slope are correlated with age. So really, the craters of the cones in Cima are getting wider relative the bases (that is, flatness increases) towards the present. The angle of slope either increases towards the present as a result of the change in flatness (since the height-to-radius ratio is constant) or decreases towards the past as a result of erosion (and coincidentally in tandem with the flatness to keep the height-to-radius ratio constant). The cause of this correlation is not obvious. Empirically, angle of slope and flatness are

Table 4
Input values for initial basal diameter (B), volume flux (Q) and flatness (f).

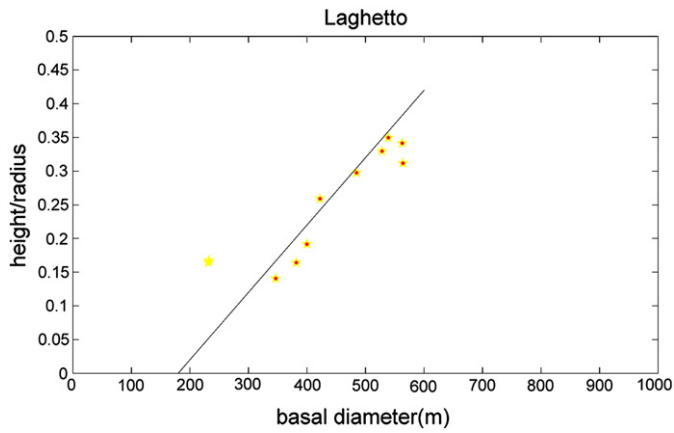| B (m)	50	70	90	100	150	190	200	250	250	270
Q (m³/s)	0.05	0.1	0.5	1	5	10	20	30	40	50
f (−)	0.1	0.15	0.2	0.25	0.3	0.35	0.4	0.45	0.5	0.55

Fig. 11. The variation in height-to-radius ratio with basal diameter was fit with a linear regression. $(h/r) = 0.001(2r) - 0.18$. The yellow stars track the growth of Cono del Laghetto during all phases. The red dots indicate which values were used in the regression; the remaining value occurred during the early phreatomagmatic phase before significant growth started.

related to each other and to the height-to-radius ratio: angle of slope is normally written as:

$$\text{angle of slope} = arctan(h / (r-t)),$$

where h = height, r = basal diameter/2, and t = top diameter/2. However, it is possible to rearrange the terms to get:

$$\text{angle of slope} = arctan((h/r) / (1-f)),$$

where h/r = height-to-radius ratio, and f = flatness = t/r. This makes it quite clear that all of the important geomorphic parameters, namely angle of slope, height-to-radius ratio and flatness, are interrelated, if one varies, one other must also vary (Fig. 9). Since the height-to-radius ratio is constant (within error) for most volcanic fields, including Cima, any

variation in angle of slope is connected to a variation in flatness. Flatness could change with explosivity due to changes in magmatic water or the presence of groundwater; the angle of slope merely responding to the change in flatness. Alternatively, the downslope movement of material could decrease angle of slope; flatness then decreases as the cone grows a sediment apron.

4.1. Historical eruptions of cinder cones

We turn now to observations of cinder cones that erupted in historical times, where scientists could measure how they grew. We consider two cones in particular: Paricutin of the MGVF in Mexico, which has been especially well studied (Luhr and Simkin, 1993) and Cono del Laghetto on the high southern flank of Mount Etna, Italy, which erupted in 2001 (Bekncke and Neri, 2003; Favalli et al., 2009; Fornaciai et al., 2010). Fig. 10 shows the change in height, basal diameter, angle of slope and flatness as these cones grew. Profiles of Paricutin were scanned from Luhr and Simkin (1993) and measured. Digital profiles of Laghetto were produced from digitized photographs taken during cone growth. In both cases, the basal diameter, top diameter and height were measured from the profiles directly. Angles of slope were both measured and calculated. Flatness is calculated from basal and top diameter.

Paricutin is a classic large cinder cone. It grew so fast it almost reached its final angle of slope in the first few days. The first profile is only 3 days after the start of the eruption and the cone has already reached an angle of slope of 33°. For most of its eruption, Paricutin maintained a constant flatness (0.25) and angle of slope (29°).

Laghetto is a much smaller cinder cone and it didn't grow as fast (or as big). Also, modern technology (airplanes and laser altimetry) allowed the collection of topographic profiles during the active eruption so we can see the early stages of cinder cone growth. During the initial phreatomagmatic phase (Bekncke and Neri, 2003; Calvari and Pinkerton, 2004), little or no growth occurred: height and basal diameter do not change much (Fig. 10b). Once the main cone growth starts, the angle of slope begins to rise quickly (from 10° to 24°) as the height and the basal diameter increase. Later in the eruption as growth tails off, the angle of slope becomes constant. The flatness is
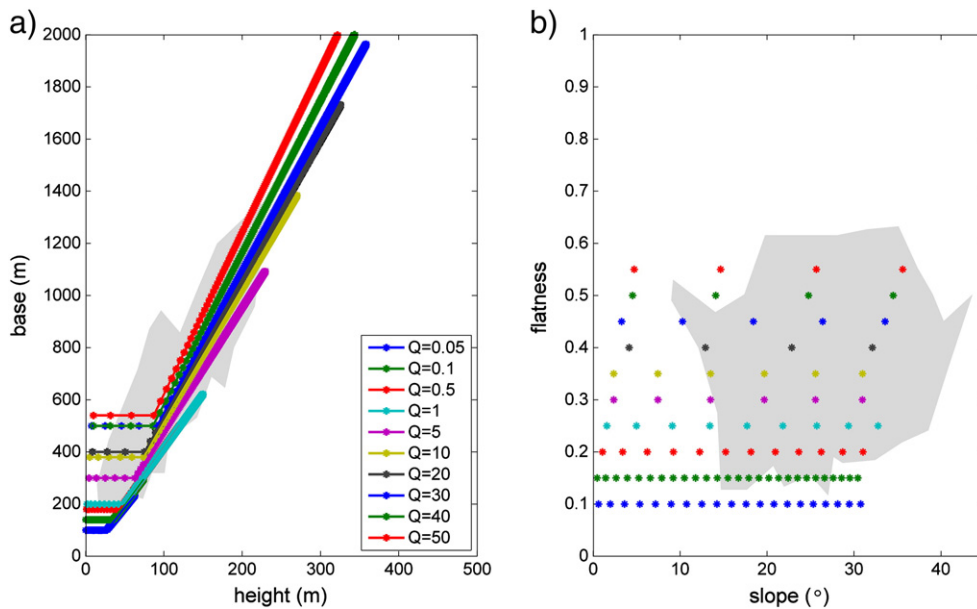

Fig. 12. The results of our numerical model of cinder growth actual show a set of growing cones (colored dots and lines) passing through the morphospace that the GSVF cones describe (light gray regions). The colors indicate the different magma fluxes used (consult Table 4 for the corresponding initial basal diameters and flatnesses). Clearly, this very simple numerical model can create cones of a wide variety of morphologies. This indicates that erosion is not necessary for cinder cones to have low angles of slope or low flatnesses. (a) Basal diameter versus height. (b) Flatness versus angle of slope.

constant throughout most of the eruption at 0.15. An ending explosion widened the crater resulting in a drop in height and increase in flatness; this final phase is ignored in the conceptual model below. Subsequent collection of topographic data using LiDAR has documented the morphology of Laghetto in detail and shown the minor alteration it has undergone in the first several years after eruption (Favalli et al., 2009; Fornaciai et al., 2010). Detailed analysis of the LiDAR data allowed the collection of angle of slope data with sufficient resolution to recognize the difference between the steepest central portion of the cone (reaching angles of slope of 29°–31°) and the shallower apron surrounding the cone. This study analyzed a set of single profiles and calculated angles of slope based on the basal diameter, top diameter and height; the lower angles of slope estimated (see Fig. 10 and Table 1) reflect partially the choice of wider base and partially the averaging effect of the calculation of angle of slope from basic measurements (as opposed to the detailed grid of slopes obtained from high-resolution LiDAR). However, our calculations better match the type of data available for other historically-erupted cones and for the populations of cinder cones in many areas of the world.

We propose a conceptual model of cinder cone growth: (1) eruption volume flux increases rapidly at first and decreases towards the end of the eruption; basal diameter and height correspondingly increase rapidly at the start of the eruption and then more slowly later in the eruption. (2) Angle of slope increases initially showing that the height increases much faster than the basal diameter in the initial stage of growth. (3) Once the angle of repose is achieved, angle of slope ceases to increase and the basal diameter and height increase together. (4) For a given cone, flatness is more or less constant. Both flatness and the angle of repose may vary between cones (due to explosivity, grain size distribution, scoria rheology and climatic factors). The initial basal diameter reflects the area over which scoria is distributed as it falls out of the sides of the eruption column; so the initial basal diameter is postulated to vary with volume flux into the cone.

We have implemented this conceptual model as a numerical model using the following three equations to constrain growth in two phases. The first equation relates the supply of magma to the volume of the cone:

$$V = Q(\exp(-t/b)/b - \exp(-t/a)/a),$$

where V is volume (in m^3), Q is the potential magma flux (in m^3/s), t is time (in s), a is a damping factor (in s) controlling the decline in volume flux at the end of the eruption, and b is a factor controlling the initial increase in volume flux. This equation combines a reasonable mathematical form for magma supply rates and mass conservations considerations (Bemis et al., 2008; Bemis et al., 2010). The two constants, a and b, were estimated as 2×10^7 s and 1×10^5 s, respectively, based on a regression of the volume flux equation with observed changes in volume at Paricutin and Cono del Laghetto. The volume flux Q is varied between model runs (see Table 4).

The second equation relates the volume of the cone to its morphology:

$$V = (1/3)r^3(h/r)\left(1 + f + f^2\right),$$

where V is again volume, r is the basal radius of the cone, h is the height of the cone, and f is the flatness of the cone. The flatness f is either held constant at 0.3 or changes with the potential magma flux. The basal radius r enters directly only in the r^3 term.

The final equation relates the steepness of the cone to the size of the cone during the first growth phase:

$$h/r = 0.001(2r) - 0.18,$$

which is based on fitting h/r to 2r for the angle of slope increasing phase of growth in Laghetto (Fig. 11). In the first growth phase, this equation

restricts growth to primarily an increase in height (with only a moderate increase in basal diameter) by forcing the cone to get steeper as it grows. During the second phase of growth, the forced increase in steepness is relaxed and the basal radius increases more rapidly.

The most interesting results of the numerical regression were obtained when the initial basal diameter, the potential magma flux and the flatness were assumed to be related. Table 4 shows how they varied together; each was constant for a single run of the model. Fig. 12 shows the results of the numerical model of cinder cone growth.

Our model is capable of growing cones in most of the morphologic space covered by the GSVF cones. The main exception is the relatively large but very low height-to-radius ratio cones in the upper left of Figs. 3b and 6b; these cones may well be modified by erosion. But most of the other cones could reflect primary morphology.

5. Conclusions

Overall, GSVF cinder cones exhibit a wide range in most geomorphic parameters, such as cone height, basal diameter (radius), angle of slope and flatness. Their height/radius (h/r) ratios, on the other hand, are generally around 0.33, essentially identical to the h/r ratios of pristine, uneroded terrestrial cinder cones. No geomorphic parameters change systematically with measured ^{40}Ar/^{39}Ar age, suggesting the morphological variance is not due to cinder cone degradation. Instead we propose that much of the variance in GSVF cinder cones reflects variable primary eruption characteristics, such as magma flux. This proposal is supported by simple numerical modeling.

In sum, cinder cone growth and erosion produce similar trends in morphologic space. Therefore, it is very important to use multiple geomorphic indicators to correctly disentangle growth from degradation.

Appendix A. Supplementary data

Supplementary data to this article can be found online at doi:10.1016/j.jvolgeores.2010.11.007.

References

Bemis, K. G., 1995. A morphometric study of volcanoes in Guatemala, Iceland, the Snake River Plain, and the South Pacific. Ph.D. Thesis, Rutgers University.
Bemis, K.G., Bonar, D.E., 1997. Models of cinder cone growth: the effects of ballistic drag and grain flow. Abstract. Symposium on Localization Phenomena and Dynamics of Brittle and Granular Systems.
Bemis, K., Borgia, A., Neri, M., 2008. Magma Supply Rates Inferred from Cinder Cone Radii. IAVCEI, Iceland. 2008 (abstract).
Bemis, K., Borgia, A., and Neri, M., 2010. Magma supply rates inferred from cinder cone radii. Forthcoming.
Bekncke, B., Neri, M., 2003. The July–August 2001 eruption of Mt. Etna (Sicily). Bulletin of Volcanology 65, 461–476.
Burkhart, B., Self, S., 1985. Extension and rotation of crustal blocks in Northern Central America and effect of the volcanic arc. Geology 13, 22–26.
Bloomfield, K., 1975. A late-Quaternary monogenetic volcano field in Central Mexico. Geologishce Rundschau 64, 476–497.
Calvari, S., Pinkerton, H., 2004. Birth, growth and morphologic evolution of the 'Laghetto' cinder cone during the 2001 Etna eruption. Journal of Volcanology and Geothermal Research 132, 225–239.
Carn, S.A., 2000. The Lamongan volcanic field, East Java, Indonesia: physical volcanology, historic activity, and hazards. Journal of Volcanology and Geothermal Research 95, 81–108.
Carr, M.J., Stoiber, R.E., 1990. Volcanism. In: Dengo, G., Case, J.E. (Eds.), The geology of North America: The Caribbean region: Geol Soc Am H, pp. 375–391.

DeMets, C., Gordon, R.G., Argus, D.F., Stein, S., 1990. Current plate motions. Geophysical Journal International 101, 425–478.

Donnelly, T.W., Horne, G.S., Finch, R.C., Lopez-Ramos, E., 1990. Northern Central America; the Maya and Chortis Block. In: Dengo, G., Case, J.E. (Eds.), The geology of North America: The Caribbean region: Geol Soc Am H, pp. 37–75.

Chouet, B., Hamisevicz, N., McGetchin, T.R., 1974. Photoballistics of volcanic jet activity at Stromboli, Italy. Journal of Geophysical Research 79, 4961–4976.

Cohen, B., Bemis, K.G., 1998. Spontaneous stratification as a possible mechanism for the formation of reverse graded layering in cinder cones (abs.): EOS, Trans. AGU, Spring Meet. Suppl., Abstract T21B-06.

Dohrenwend, J.C., Wells, S.G., Turrin, B.D., 1986. Degradation of Quaternary cinder cones in the Cima volcanic field, Mojave Desert, California. Geological Society of America Bulletin 97, 421–427.

Favalli, M., Karatson, D., Mazzarini, F., Pareschi, M.T., Boschi, E., 2009. Morphometry of scoria cones located on a volcano flank: a case study from Mt. Etna (Italy), based on high-resolution LiDAR data. Journal of Volcanology and Geothermal Research 183, 320–330.

Fedotov, S.A., Markhinin, Ye.K. (Eds.), 1983. The Great Tolbachik Fissure Eruption: Geological and Geophysical Data 1975–1976. Cambridge University Press, Cambridge, England.

Fornaciai, A., Behncke, B., Favalli, M., Neri, M., Tarquini, S., Boschi, E., 2010. Detecting short-term evolution of Etnean cinder cones: a LIDAR-based approach. Bulletin of Volcanology. doi:10.1007/s00445-010-0394-3.

Hasenaka, T., Carmichael, I.S.E., 1985a. The cinder cones of Michoacán–Guanajuato, Central Mexico: their age, volume and distribution, and magma discharge rate. Journal of Volcanology and Geothermal Research 25, 105–124.

Hasenaka, T., Carmichael, I.S.E., 1985b. A compilation of location, size, and geomorphological parameters of volcanoes of the Michoacan–Guanajuato volcanic field, central Mexico. Geofisica Internacional 24–4, 577–607.

Hooper, D. M., 1994. Geomorphologic modeling of the degradational evolution of cinder cones. PhD dissertation, State University of New York at Buffalo, Buffalo, NY, 312 pp.

Hooper, D.M., Sheridan, M.F., 1998. Computer-simulation models of scoria cone degradation. Journal of Volcanology and Geothermal Research 83, 241–267.

Kervyn, M., Ernst, G., Carracedo, J.-C., Jacobs, P., 2010. Geomorphology of "monogenetic" volcanic cones, submitted to Geomorphology.

Luhr, J.F., Simkin, T. (Eds.), 1993. Paricutin, the Volcano Born in a Mexican Cornfield. Geoscience Press, Inc., Phoenix. 427 pp.

McGetchin, T.R., Settle, M., Chouet, B.A., 1974. Cinder cone growth modeled after Northeast crater, Mount Etna, Sicily. Journal of Geophysical Research 79, 3257–3272.

Porter, S.C., 1972. Distribution, morphology, and size distribution of cinder cones on Mauna Lea Volcano, Hawaii. Geological Society of America Bulletin 83, 3607–3612.

Riedel, C., Ernst, G.G.J., Riley, M., 2003. Controls on the growth and geometry of pyroclastic constructs. Journal of Volcanology and Geothermal Research 127, 121–152.

Settle, M., 1979. The structure and emplacement of cinder cone fields. American Journal of Science 279, 1089–1107.

Smith, D.K., Cann, J.R., 1992. The role of seamount volcanism in crustal construction at the Mid-Atlantic Ridge (24°–30°N). Journal of Geophysical Research 97, 1645–1658.

Turrin, B.D., Dohrenwend, J.C., Wells, S.G., McFadden, L.D., 1984. Geochronology and eruptive history of the Cima volcanic field, eastern Mojave Desert, California: Geological Society of America 1984 Annual Meeting Guidebook, Reno, Nevada, field trip 14, 88–100.

Turrin, B.D., Dohrenwend, J.C., Drake, R.E., Curtis, G.H., 1985. Potassium–argon ages from the Cima volcanic field, eastern Mojave Desert, California. Isochron West 44, 9–16.

Turrin, B.D., Donnelly-Nolan, J.M., Hearn, B.C., 1994. ^{40}Ar/^{39}Ar ages from the rhyolite of Alder Creek, California: age of the Cobb Mountain normal-polarity subchron revisited. Geology 22, 251–254.

Turrin, B.D., Christiansen, R.L., Clynne, M.A., Champion, D.E., Gerstel, W.J., Muffler, L.J.P., Trimble, D.A., 1998. Age of Lassen Peak, California, and implications for the ages of late Pleistocene glaciations in the southern Cascade Range. Geol. Soc. Amer. Bull. 110, 931–945.

Walker, J.A., Singer, B.S., Jicha, B.R., Cameron, B.I., Carr, M.J., Olney, J.L., 2011. Monogenetic, behind-the-front volcanism in southeastern Guatemala and western El Salvador: ^{40}Ar/^{39}Ar ages and tectonic implications. Lithos 123, 243–253.

Williams, H., McBirney, A.R., Dengo, G., 1964. Geologic Reconnaissance of Southeastern Guatemala. University of California Press, Berkeley and Los Angeles.

Wood, C. A., 1979. Morphometric studies of planetary landforms: impact craters and volcanoes. Ph.D. Thesis: Brown University.

Wood, C.A., 1980a. Morphometric evolution of cinder cones. Journal of Volcanology and Geothermal Research 7, 387–413.

Wood, C.A., 1980b. Morphometric analysis of cinder cone degradation. Journal of Volcanology and Geothermal Research 8, 137–160.